ISSN 2096-7071
CN 10-1629/R1

CHINA CDC WEEKLY

Vol. 4 No. 31 Aug. 5, 2022

中国疾病预防控制中心周报

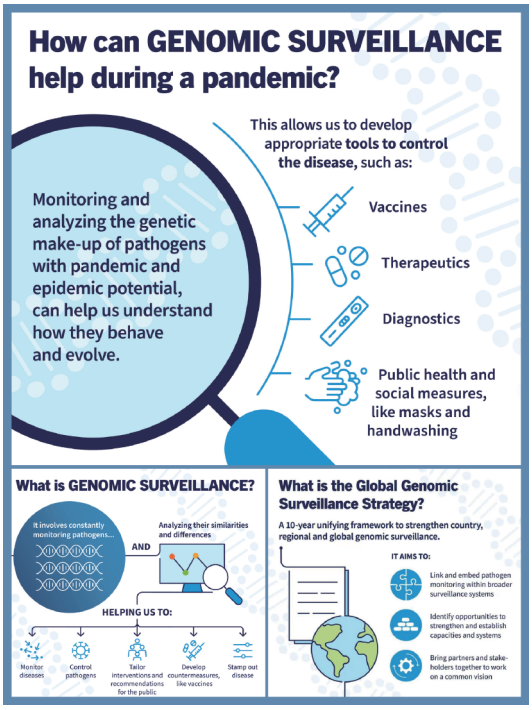

COVID-19 ISSUE (29)

ISSN 2096-7071

China CDC Weekly

Cover Image: adapted from the World Health Organization, https://www.who.int/initiatives/genomic-surveillance-strategy#.

Preplanned Studies

City-Specific Effects of Lifting Mobility Restrictions — China, February–March 2020

Shasha Han[1,2]; Libing Ma[2,3]; Ting Zhang[2]; Luzhao Feng[2]; Weizhong Yang[2]; Xiaoying Zheng[2,#]

Summary

What is already known about this topic?

Government used mobility restrictions to help contain the first wave of coronavirus disease 2019 (COVID-19) across cities in China. The restrictions were lifted during times of non-zero incidence in response to a return to work order that went into effect on February 10, 2020.

What is added by this report?

The effect of lifting mobility restrictions on COVID-19 death rate and incidence varied by city, with smaller increases or even reductions in cities with low community connectivity and small floating volume, and larger increases in cities with high community connectivity and large floating volume. Effects on recovery rates were similar across cities.

What are the implications for public health practice?

City-specific mobility restriction lifting is likely to be beneficial. Two indexes, community connectivity and floating volume, can inform the design of city-specific mobility restriction lifting policies.

Human mobility restrictions have shown to be effective in mitigating the spread of severe acute respiratory syndrome coronavirus 2 (SARS-CoV-2) transmission (*1–2*). However, mobility restrictions disrupt social and economic activities (*3–4*), threatening fiscal revenues for national and local governments (*5*) and affecting mental health of individuals (*6*). Mobility restrictions were frequently lifted during times of non-zero coronavirus disease 2019 (COVID-19) incidence, although evidence suggests this may increase virus transmission (*7–8*). A deeper understanding of the impact of lifting mobility restrictions can lead to better mitigation policies and enable policymakers to tailor reopening strategies for maximum public health benefits.

We investigated the effects of lifting mobility restrictions in 14 cities in China. We used human mobility data to model the lifting of mobility restrictions and the contrast-specific propensity score methods to control measured confounding. We found that the impacts of increased mobility on COVID-19 epidemiological outcomes could vary by city. Furthermore, we created two city vitality indexes, community connectivity and floating volume, that are useful for informing mobility lifting policies tailored to cities.

The 14 cities are three municipalities, Beijing, Shanghai, and Tianjin; five capital cities, Chengdu, Guangzhou, Hangzhou, Nanjing, and Xiamen; and six typical labor-service importing cities, Dongguan, Foshan, Ningbo, Shenzhen, Suzhou, and Wuxi. Because vaccination may confound the effect of lifting restrictions, we limited our analyses to the first wave of COVID-19, which occurred before vaccines were available.

Epidemiological data, including the laboratory-confirmed cases, recovered cases, and deaths were obtained from the health commissions of 15 city-level administrative divisions (*9*). Recovery rates were estimated as recovered cases divided by confirmed infections 15 days earlier; death rates were estimated as deaths divided by confirmed infections 14 days earlier (*10*). Social-demographic data were obtained from the China City Statistical Yearbook 2018 (*11*) and included number of employees, household population density, housing density, average number of people per household, total number of passengers, gross domestic product (GDP), number of companies, number of hospitals, number of schools, number of hospital beds, and number of physicians.

We used two factor interventions to represent the lifting of mobility restrictions. Factor 1 denoted the lifting of the intercity mobility restrictions, and Factor 2 the lifting of the intracity mobility restrictions. We dichotomized continuous intercity and intracity mobility intensities and obtained the two binary factors: 1 for lifting restrictions (low intensities) and 0 for imposing restrictions (high intensities). Intercity mobility intensity was estimated using the Baidu migration data on migration strength across cities. Day

1 was the first reopening day (February 10, 2020) and Day *n* was the *n*th day after February 10, 2020. We estimated the intercity mobility intensity as the proportions of returning population floating on Day *n*, i.e., the sum of net flow-in strength from lunar date January 3 to Day *n* divided by the net flow-out from the city during the 2020 Spring Festival holiday. Intracity mobility intensity was estimated using the Baidu migration data movement strength within cities, with three-day moving averages to smooth weekend variation. Estimated mobility intensities were dichotomized using their medians across cities and days.

We created two indexes — community connectivity and floating volume — to characterize the vitality of a city. The two indexes capture the floating and fixed aspects of a city. Community connectivity reflects the interactions of floating and fixed populations, and floating volume describes the relative population flow in space. They are defined as follows:

Community connectivity

$$\propto \frac{\text{The number of employees} \times \text{The size of household population}}{\text{City area}} = \text{The number of employees} \times \text{household population density}, \quad (1)$$

Floating volume

$$\propto \text{The number of employees} \times \text{City area} \times \frac{\text{The number of employees}}{\text{The size of household population}} = \frac{\text{The number of employees}^2}{\text{Household population density}}. \quad (2)$$

As shown above, community connectivity is proportional to the number of employees and the household population density in a city. Floating volume is proportional to the number of employees squared and inversely proportional to the household population density.

Baseline covariates include the two indexes, social-demographic characteristics, cluster of first reported cases, numbers of cases, death rates, and recovery rates before reopening.

We adopted the potential outcome framework for causal inferences and considered a city on a particular day as a unit (*12*). Because the potential outcomes of lifting for a given city on a specific day may not be independent of the outcomes for the same city on previous days, the conventional stable unit treatment value assumption is not applicable (*13*). We therefore imputed potential outcomes based on a short timeframe using the autoregressive integrated moving average model (*14*). We used the contrast-specific propensity score approach to balance groups of units for comparison, using the subclassification method that grouped units into five classes (*15*). We estimated the effects of lifting intercity mobility restrictions alone, intracity mobility restrictions alone, and the two restrictions simultaneously, within and across classes. The average effect across classes was calculated as the weighted average of causal effects across the five subclasses, with weights given by the proportions of samples within classes over the size of full samples. All the analyses were conducted using R (version 4.0.3, R Foundation for Statistical Computing, Vienna, Austria).

The three types of lifting — lifting intercity restrictions alone, intracity restrictions alone, and intercity and intracity restrictions simultaneously — increased recovery rates by 0.24 [95% confidence interval (CI): 0.23–0.26], 0.20 (95% CI: 0.19–0.22), and 0.21 (95% CI: 0.19–0.23), respectively. The three liftings increased death rates but with smaller values and wider confidence intervals, 0.09×10^{-2} (95% CI: 0.07×10^{-2}–0.11×10^{-2}), 0.03×10^{-2} (95% CI: 0.02×10^{-2}–0.05×10^{-2}) and 0.04×10^{-2} (95% CI: 0.02×10^{-2}–0.05×10^{-2}). Similarly, the three types of lifting increased cases with wider confidence intervals, 3.49 (95% CI: 2.87–4.12), 2.50 (95% CI: 2.12–2.88), and 2.22 (95% CI: 1.89–2.55). The effects of lifting on cases and death rates had large ratios of variances to means, suggesting that these effects were likely to be heterogeneous across cities.

We found that the effects of the three types of lifting on death rates varied greatly across the five classes (Figures 1–3). For example, lifting intercity restrictions reduced the death rates for cities in Class 1 (mean -0.02×10^{-2}, 95% CI: -0.03×10^{-2} to -0.01×10^{-2}) while significantly increased death rates for cities in Class 4 and 5 (Figure 1A). Lifting of intracity restrictions also showed heterogeneous effects across classes. While the liftings significantly increased death rates for cities in Class 2 by 0.06×10^{-2} (95% CI: 0.02×10^{-2}–0.11×10^{-2}), it did not impact death rates for cities in Class 5 (Figure 2A). Note that Class 5

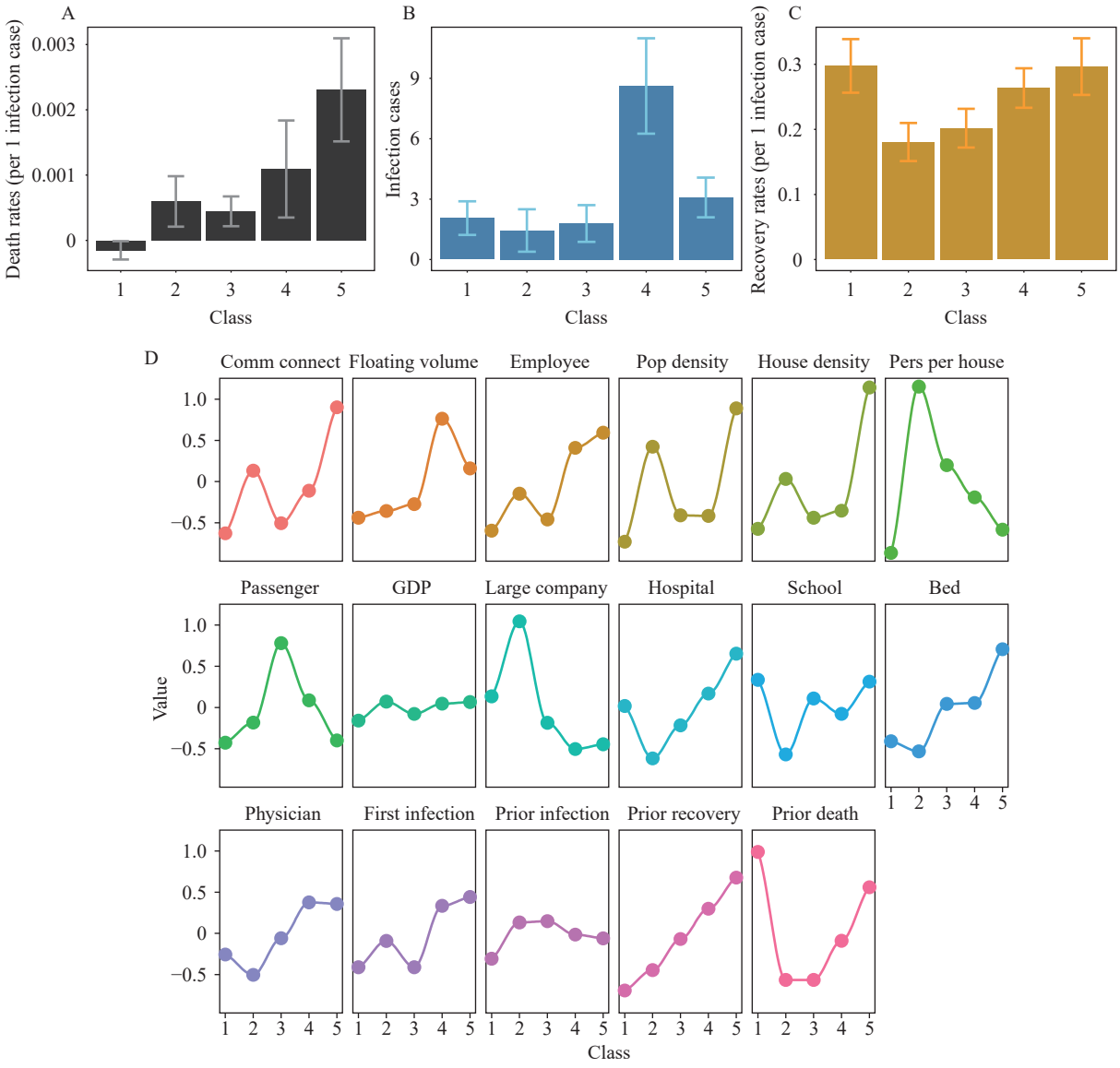

FIGURE 1. The within-class effects (means and 95% confidence interval) of lifting intercity mobility restrictions. (A) Effects in death rates for Class 1–5; (B) Effects in recovery rates for Class 1–5; (C) Effects in infection cases for Class 1–5; (D) Standardized means of city characteristics for Class 1–5.
Note: "Comm connect," the index of community connectivity; "Floating volume," the index of floating volume; "Employee," the number of employees; "Pop density," the household population density; "House density," the house density; "Pers per house," the number of persons per house; "GDP," the gross domestic product; "Large company," the number of large-size companies; "Hospital," the number of hospitals; "School," the number of schools; "Bed," the number of hospital beds; "Physician," the number of physicians; "First infection," the number of first reported infections; "Prior infection," "Prior recovery," and "Prior death," represent the infection cases, recovery rates, death rates before the effective date of the return to work order.

when investigating the contrast with lifting intra-city restrictions (Figure 2A) and when investigating the contrast with lifting intercity restrictions (Figure 1A) may consist of different cities because classes for the different contrasts were constructed under different contrast-specific propensity scores. Finally, simultaneous lifting of intercity and intracity showed zero effect for cities in Class 3 and 4 but had an increase of 0.07×10^{-2} (95% CI: 0.03×10^{-2} to -0.11×10^{-2}) in death rates for cities in Class 2 (Figure 3A). The increases in cases showed high variation across classes of cities, though all three types of lifting increased cases significantly.

To identify the factors that drove differences in deaths and cases across classes, we calculated the correlations between within-class standardized

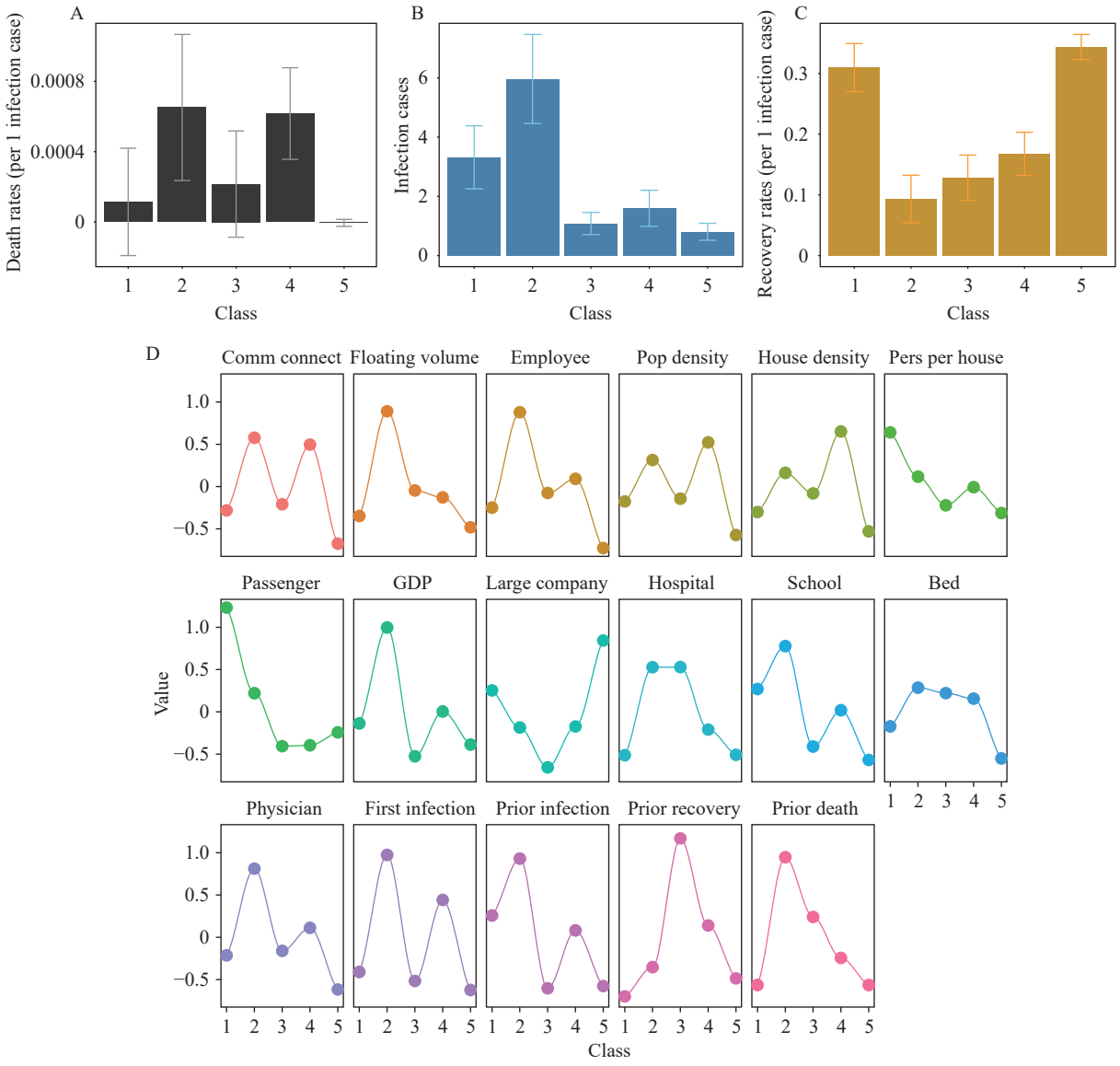

FIGURE 2. The within-class effects (means and 95% confidence interval) of lifting intracity mobility restrictions. (A) Effects in death rates for Class 1–5; (B) Effects in recovery rates for Class 1–5; (C) Effects in infection cases for Class 1–5; (D) Standardized means of city characteristics for Class 1–5.
Note: "Comm connect", the index of community connectivity; "Floating volume", the index of floating volume; "Employee", the number of employees; "Pop density", the household population density; "House density", the house density; "Pers per house", the number of persons per house; "GDP", the gross domestic product; "Large company", the number of large-size companies; "Hospital", the number of hospitals; "School", the number of schools; "Bed", the number of hospital beds; "Physician", the number of physicians; "First infection", the number of first reported infections; "Prior infection", "Prior recovery" and "Prior death," represent the infection cases, recovery rates, death rates before the effective date of the return to work order.

covariate means (Figures 1–3D) and the within-class effects. We found that community connectivity was highly correlated with the effects on death, regardless of the type of lifting. Pearson correlation coefficients between the two variables were 0.93 (P<0.05), 0.99 (P<0.05), and 0.99 (P<0.05) for lifting the intercity restrictions, the intra-city restrictions, and the two restrictions simultaneously. Floating volume was moderately correlated with the effects in cases, with Pearson correlation coefficients of 0.95 (P<0.05), 0.82 (P=0.08), and 0.90 (P<0.05) for the three types of lifting.

DISCUSSION

Although lifting mobility restrictions increased cases

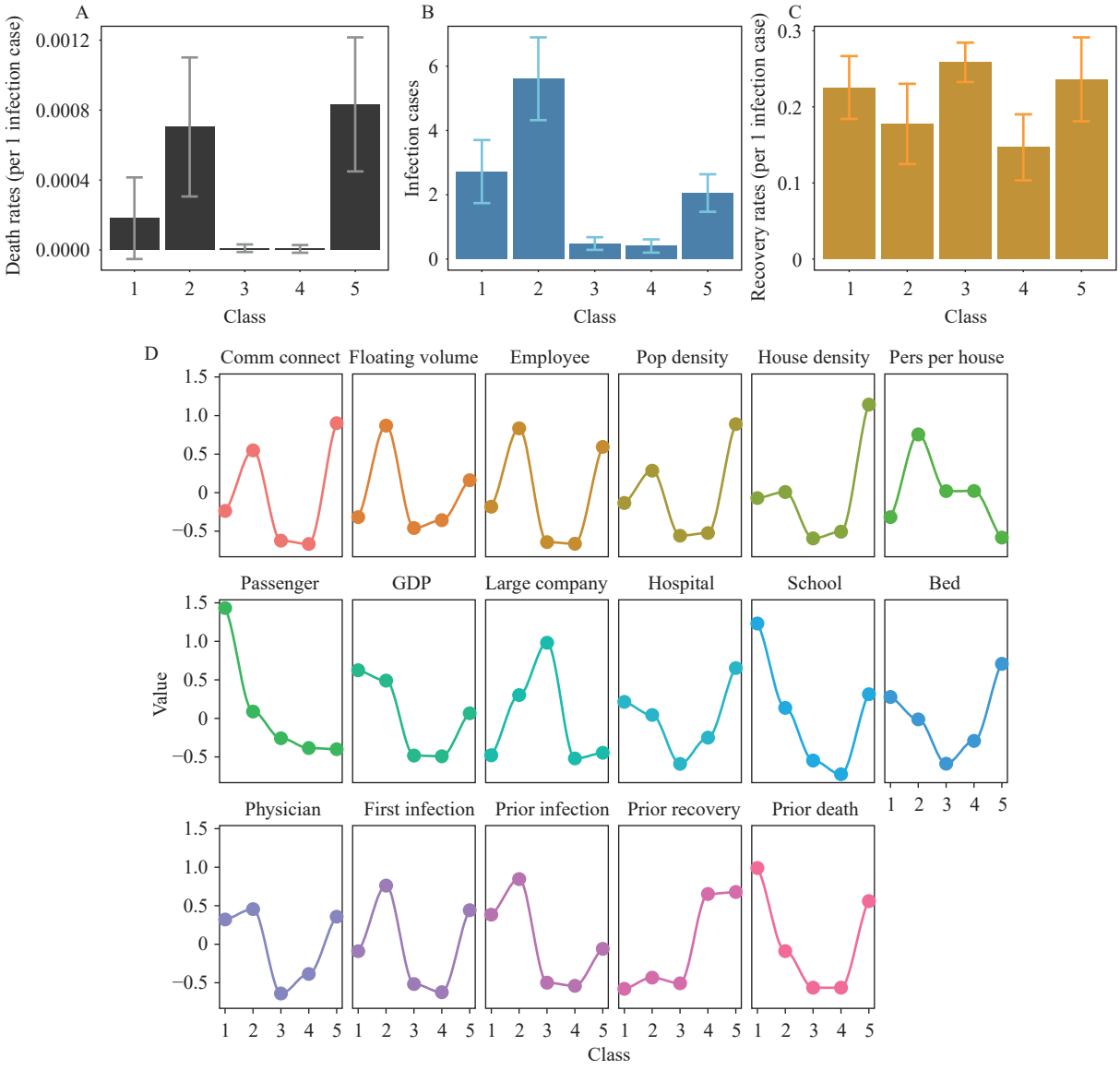

FIGURE 3. The within-class effects (means and 95% confidence interval) of simultaneously lifting intercity and intracity mobility restrictions. (A) Effects in death rates for Class 1–5; (B) Effects in recovery rates for Class 1–5; (C) Effects in infection cases for Class 1–5; (D) Standardized means of city characteristics for Class 1–5.
Note: "Comm connect," the index of community connectivity; "Floating volume," the index of floating volume; "Employee," the number of employees; "Pop density," the household population density; "House density," the house density; "Pers per house," the number of persons per house; "GDP," the gross domestic product; "Large company," the number of large-size companies; "Hospital," the number of hospitals; "School," the number of schools; "Bed," the number of hospital beds; "Physician," the number of physicians; "First infection," the number of first reported infections; "Prior infection," "Prior recovery," and "Prior death," represent the infection cases, recovery rates, death rates before the effective date of the return to work order.

and death rates for an average city, the effects varied greatly across cities. Death rates in certain cities even declined as a consequence of lifting. Nonetheless, the liftings showed similar increases in recovery rates across cities, regardless of the types of lifting. We created two indexes — community connectivity and floating volume — as predictors of the variations in effects across cities for death rates and infections, respectively.

Community connectivity is proportional to the number of employees and the household population density in a city. The lower the community connectivity, the smaller the increase in death rate. When cities had fewer employees and lower population densities, all three types of lifting would not impact or even reduce death rates while increasing recovery rates (e.g., Class 5 in Figure 1, Class 5 in Figure 2, and Class

4 in Figure 3). For two cities with the same population density, the one with fewer employees would have smaller increases in death rates (e.g., Class 3 versus 4, Figure 1A). Furthermore, given the same number of employees, cities with lower population densities would experience small or negligible increases in death rates after lifting restrictions (e.g., Class 4 versus 5, and Class 1 versus 2, Figure 1A).

Floating volume is proportional to the number of employees squared and inversely proportional to the household population density. High floating volume predicts large increases in infections upon lifting restrictions. As such, cities with both a large number of employees and a low population density would have a large increase in infections when lifting restrictions (e.g., Class 4 in Figure 1). Given the same population density, cities with more employees would have larger increases in infections (e.g., Class 3 versus 4, Figure 1B). Of note, the number of employees plays a dominant role in determining the degree of increase because the floating volume is proportional to the square of the number of employees. Thus, cities with high population densities could still experience large increases in infections if the number of employees is large (e.g., Class 2 in Figure 2).

Finally, high community connectivity and floating volume predict large increases in both deaths and infections upon lifting restrictions (e.g., Class 2 in Figures 2 and 3).

Our results highlight the need for city-specific lifting strategies in China. Policies targeting the two indexes need to accompany the lifting of mobility restrictions to control death rates and infections. Cities with high community connectivity should consider flexible working strategies (e.g., rotating schedules, shift work, and job-sharing) and provide less dense living places for floating populations. Cities with high floating volume and community connectivity should ensure sufficient healthcare resources to care for severely ill patients prior to lifting mobility restrictions.

To properly interpret our findings, it is important to consider the study's limitations. While we have reduced confounding due to vaccination by restricting the study to the first wave of the COVID-19 pandemic, which occurred before COVID-19 vaccines were available, there may exist confounding due to urbanization. We used the number of employees, large-size companies, hospitals, hospital beds, and physicians as proxies for urbanization, but these factors may not fully capture urbanization. Second, since the SARS-CoV-2 strain circulating during the first wave of the COVID-19 pandemic had slower transmission and higher infection fatality rates than the Omicron variant, our estimated effects cannot be directly extrapolated to the current situation. However, because the variants are transmitted in similar ways, the factors for predicting effect differences are likely to remain the same. Furthermore, the effects of lifting restrictions may be influenced by age distribution and presence of chronic health conditions in citizens. More sophisticated indexes that are able to account for these features are needed. Finally, future research could continue to explore the causal pathways of how increased mobility affects epidemiological outcomes. For example, increased access to ventilators and other medical resources as well as food supplies, which the lifting of mobility restrictions may influence, could play a mediator role.

Our study provides a unique perspective on factors that drive the heterogeneous effects of lifting mobility levels in cities. A comprehensive understanding of these factors is crucial so cities can prepare properly for lifting their mobility restrictions.

Conflicts of interest: No conflicts of interest.

Funding: Supported by grants from the Chinese Academy of Medical Sciences Innovation Fund for Medical Sciences (2020-I2M-1-001); Non-profit Central Research Institute Fund of Chinese Academy of Medical Sciences(2021-RC330-002); and Guilin talent mini-highland scientific research project for COVID-19 prevention and control (Municipal Committee Talent Office of Guilin City [2020] No. 3-05).

doi: 10.46234/ccdcw2022.142

[#] Corresponding author: Xiaoying Zheng, xzheng@pku.edu.cn.

[1] Beijing International Center for Mathematical Research, Peking University, Beijing, China; [2] School of Population Medicine and Public Health, Chinese Academy of Medical Sciences & Peking Union Medical College, Beijing, China; [3] Department of Respiratory and Critical Care Medicine, the Affiliated Hospital of Guilin Medical University, Guilin City, Guangxi Zhuang Autonomous Region, China.

Submitted: June 10, 2022; Accepted: July 27, 2022

REFERENCES

1. Haug N, Geyrhofer L, Londei A, Dervic E, Desvars-Larrive A, Loreto V, et al. Ranking the effectiveness of worldwide COVID-19 government interventions. Nat Hum Behav 2020;4(12):1303 – 12. http://dx.doi.org/10.1038/s41562-020-01009-0.
2. Tian HY, Liu YH, Li YD, Wu CH, Chen B, Kraemer MUG, et al. An investigation of transmission control measures during the first 50 days of the COVID-19 epidemic in China. Science 2020;368(6491):638 – 42. http://dx.doi.org/10.1126/science.abb6105.
3. Chetty R, Friedman JN, Hendren N, Stepner M, The Opportunity

Insights Team. The economic impacts of COVID-19: evidence from a new public database built using private sector data. 2020 Jun. NBER Working Paper No. w27431. https://www.nber.org/papers/w27431.
4. Guan DB, Wang DP, Hallegatte S, Davis SJ, Huo JW, Li SP, et al. Global supply-chain effects of COVID-19 control measures. Nat Hum Behav 2020;4(6):577 – 87. http://dx.doi.org/10.1038/s41562-020-0896-8.
5. Bonaccorsi G, Pierri F, Cinelli M, Flori A, Galeazzi A, Porcelli F, et al. Economic and social consequences of human mobility restrictions under COVID-19. Proc Natl Acad Sci USA 2020;117(27):15530 – 5. http://dx.doi.org/10.1073/pnas.2007658117.
6. Gimbrone C, Rutherford C, Kandula S, Martínez-Alés G, Shaman J, Olfson M, et al. Associations between COVID-19 mobility restrictions and economic, mental health, and suicide-related concerns in the US using cellular phone GPS and Google search volume data. PLoS One 2021;16(12):e0260931. http://dx.doi.org/10.1371/journal.pone.0260931.
7. Hatchett RJ, Mecher CE, Lipsitch M. Public health interventions and epidemic intensity during the 1918 influenza pandemic. Proc Natl Acad Sci USA 2007;104(18):7582 – 7. http://dx.doi.org/10.1073/pnas.0610941104.
8. Chowell G, Echevarría-Zuno S, Viboud C, Simonsen L, Tamerius J, Miller MA, et al. Characterizing the epidemiology of the 2009 influenza A/H1N1 pandemic in mexico. PLoS Med 2011;8(5):e1000436. http://dx.doi.org/10.1371/journal.pmed.1000436.
9. National Health Commission of the People's Republic of China. Latest situation on the COVID-19. 2022. http://www.nhc.gov.cn/cms-search/xxgk/getManuscriptXxgk.htm?id=0c63639099e64612993590e0b2b329e8. [2022-5-31]. (In Chinese).
10. Baud D, Qi XL, Nielsen-Saines K, Musso D, Pomar L, Favre G. Real estimates of mortality following COVID-19 infection. Lancet Infect Dis 2020;20(7):773. http://dx.doi.org/10.1016/S1473-3099(20)30195-X.
11. National Bureau of Statistics of China. China Statistical Yearbook 2018. 2018. http://www.stats.gov.cn/tjsj/ndsj/2018/indexeh.htm. [2020-6-20]. (In Chinese).
12. Imbens GW, Rubin DB. Causal inference for statistics, social, and biomedical sciences: an introduction. Cambridge: Cambridge University Press. 2015. http://dx.doi.org/10.1017/CBO9781139025751.
13. Basu D. Randomization analysis of experimental data: the fisher randomization test. J Am Stat Assoc 1980;75(371):575 – 82. http://dx.doi.org/10.1080/01621459.1980.10477512.
14. Rubin DB, Stroud TWF. Bayesian break-point forecasting in parallel time series, with application to university admissions. Can J Stat 1987;15(1):1 – 19. http://dx.doi.org/10.2307/3314857.
15. Han SS, Rubin DB. Contrast-specific propensity scores. Biostat Epidemiol 2021;5(1):1 – 8. http://dx.doi.org/10.1080/24709360.2021.1936421.

Vital Surveillances

Genomic Surveillance for SARS-CoV-2 Variants of Concern from Imported COVID-19 Cases — the Mainland of China, 2021

Yenan Feng[1,2,&]; Xiang Zhao[1,2,&]; Zhixiao Chen[1]; Kai Nie[1,2]; Zeyuan Yin[1]; Ying Xia[1]; Ji Wang[1,2]; Peihua Niu[1,2]; Ruhan A[1]; Lili Li[1]; Dayan Wang[1]; Wenjie Tan[1]; Xuejun Ma[1,2]; Shiwen Wang[1,2]; Huanyu Wang[1]; George F. Gao[1,2]; Cao Chen[1,2,#]; Wenbo Xu[1,2,#]

ABSTRACT

Introduction: After the epidemic in Wuhan City was brought under control in 2020, local outbreaks of coronavirus disease 2019 (COVID-19) in the mainland of China were mainly due to imported COVID-19 cases. The ongoing evolution of severe acute respiratory syndrome coronavirus 2 (SARS-CoV-2) has continued to generate new variants. Some have been designated as variants of concern (VOCs) by the World Health Organization (WHO). To better assess the role of imported SARS-CoV-2 surveillance and the prevalence of VOCs in 2021, the genomic surveillance data of SARS-CoV-2 from imported COVID-19 cases of 2021 in the mainland of China were analyzed.

Methods: The analyses included the number of sequence submissions, time of sequence deposition, and time of detection of the VOCs in order to determine the timeliness and sensitivity of the surveillance. The proportions of VOCs were analyzed and compared with data from the Global Initiative of Sharing All Influenza Data (GISAID).

Results: A total of 3,355 sequences of imported cases were submitted from 29 provincial-level administrative divisions, with differences in the number of sequence submissions and median time of sequence deposition. A total of 2,388 sequences with more than 90% genomic coverage were used for lineage analysis. The epidemic trend from Alpha to Delta to Omicron in imported cases was consistent with that in the GISAID. In addition, VOCs from imported cases were usually identified after WHO designation and before causing local outbreaks.

Conclusions: The global distribution of SARS-CoV-2 VOCs changed rapidly in 2021. Robust genomic surveillance of the imported SARS-CoV-2 in the mainland of China is of great significance.

Severe acute respiratory syndrome coronavirus 2 (SARS-CoV-2), the etiological agent of coronavirus disease 2019 (COVID-19), is constantly mutating under the different circumstances of global transmission (*1*). The emerging SARS-CoV-2 variants may have potential adverse impacts on epidemic traits and severity. To some extent, it is also capable of escaping natural and vaccine-induced immunity (*2*–*3*). Some of them were designated as variants of concern (VOCs) by the World Health Organization (WHO) (*4*). Therefore, robust surveillance is essential to assess the evolution of viruses in real time.

After the epidemic in Wuhan City was brought under control in 2020, several COVID-19 outbreaks in the mainland of China have been proven to relate to SARS-CoV-2 contaminated cold-chain products (*5*–*7*), while most were caused by transmission through imported cases on flights, at isolation facilities, or in designated hospitals (*8*–*9*). Therefore, genomic surveillance for SARS-CoV-2 from imported cases is of great significance for monitoring the risk of different variants that were imported into the mainland of China, assessing the risk of importation-associated domestic spread, and helping guide public health interventions. On March 17, 2020, the China CDC released a notice and launched genomic surveillance for SARS-CoV-2 from imported COVID-19 cases nationwide. The laboratories of provincial CDCs were required to conduct SARS-CoV-2 whole-genome sequencing for samples from imported cases and submit the genomic sequences to the China CDC in time. This study includes the analysis of genomic surveillance data of imported SARS-CoV-2 cases of 2021 from the mainland of China.

METHODS

The sequences of SARS-CoV-2 from laboratories of the provincial CDC were submitted to the China CDC for verification and further analyses. Data from

Hong Kong Special Administrative Region (SAR), China, Macao SAR, China, and Taiwan, China were not included in this study. Global SARS-CoV-2 sequence surveillance data were collected from the Global Initiative of Sharing All Influenza Data (GISAID) up to March 9, 2022.

Spatial mapping was conducted to describe the regional distribution of SARS-CoV-2 sequences from imported COVID-19 cases and the timeliness of sequence submission. The standard map [No. GS (2016) 2923] was downloaded without modification from the standard map service website of the National Administration of Surveying, Mapping and Geographic Information. Lineage analysis was conducted on sequences with genomic coverage above 90%. SARS-CoV-2 lineages were assigned using the Phylogenetic Assignment of Named Global Outbreak Lineages web application (PANGOLIN; version 4.0.5) (*10*). The SARS-CoV-2 VOCs were classified according to the WHO's designation (*4*). The proportions of VOCs were calculated based on the date of sample collection. As it takes several days to weeks from sample collection to sequence submission, the number of submitted sequences in December was lower than the actual value.

RESULTS

The SARS-CoV-2 genomic sequences of 3,355 imported COVID-19 cases were submitted to the China CDC from January 1 to December 31, 2021 (upon validation, one sequence of them was submitted on December 25, 2020). Except for Xizang (Tibet) Autonomous Region and Qinghai Province, the remaining provincial-level administrative divisions (PLADs) had sequences submitted in various amounts (Figure 1A). The 3 PLADs with the largest submitted sequences were Shanghai Municipality (23.9%, 803/3,355), Yunnan Province (22.9%, 768/3,355), and Guangdong Province (16.9%, 568/3,355), followed by Tianjin Municipality, Fujian Province, Sichuan Province, and Henan Province, which submitted more than 100 sequences each. There were 8 PLADs that submitted 30–100 sequences. The remaining 14 PLADs submitted fewer than 30 sequences each.

To validate the timeliness of the sequence submission, the deposition time of each sequence was calculated according to the date of sample collection and sequence submission. The results showed that Shaanxi Province had the longest median time of sequence deposition with 67 days (Q_3-Q_1=109-8), followed by Fujian with 23 days (Q_3-Q_1=44-11). The remaining PLADs submitted sequences within 3 weeks of sample collection (Figure 1B).

Of the 3,355 sequences, 3,309 sequences were collected in 2021. Of the 3,309 sequences, 2,388 (72.2%) had a genomic coverage of >90%, allowing for

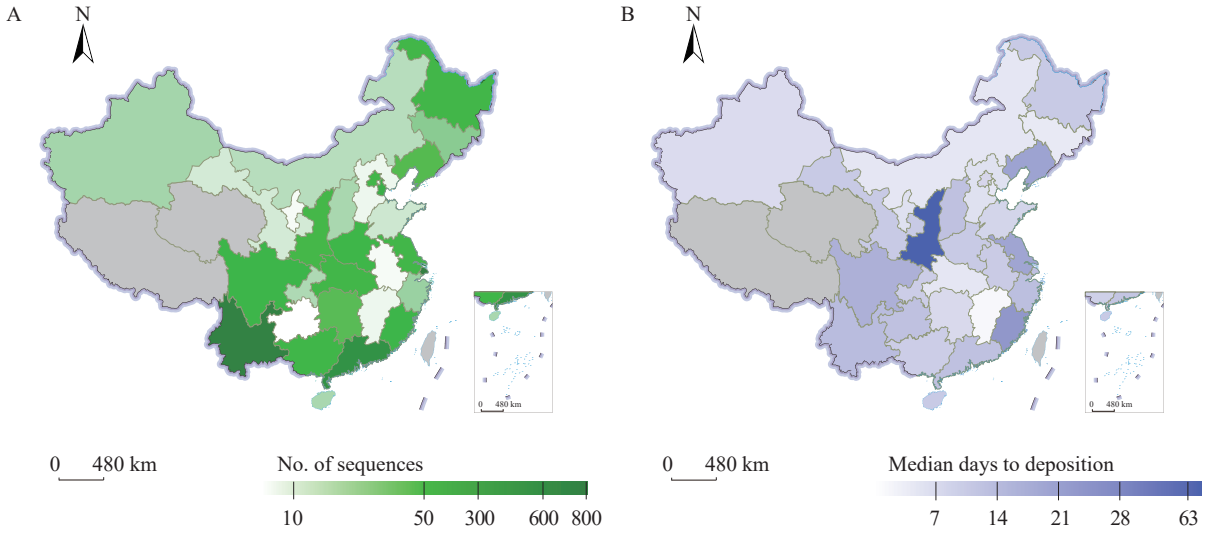

FIGURE 1. The surveillance of SARS-CoV-2 genome of imported cases in the mainland of China, 2021. (A) The number of genomic sequences of imported cases submitted by PLADs. (B) The median sequence deposition time of each PLAD from sample collection to sequence submission.
Note: Data as of December 31, 2021. Grey part means no data.
Abbreviation: SARS-CoV-2=severe acute respiratory syndrome coronavirus 2; PLAD=provincial-level administrative division.

further lineage analysis (Figure 2A). From January to April, the number of submitted sequences was less than 100 available sequences per month. Since May, the number had increased, with more than 100 available sequences per month. July and August had the highest numbers, with 548 and 407 available sequences, respectively. All five VOCs (Alpha, Beta, Gamma, Delta, and Omicron) were identified in the imported cases. The proportion of the Alpha variant was the highest from February to May. Subsequently, the Delta variant gradually replaced Alpha, becoming dominant in June and overwhelmingly dominant from August to November (more than 95% per month). In December, Omicron variants were detected, accounting for 54.3% (151/278) of the sequences, including BA.1 and BA.2 lineages.

The pattern of prevalence of the VOCs from the imported SARS-CoV-2 surveillance was similar to that in GISAID (Figure 2B). However, the relative proportions of VOCs were different, particularly for the Beta and Gamma variants. From January to May, the proportion of the Beta variant in the imported SARS-CoV-2 surveillance was more than 10% per month, compared to the data of 1.2%–2.2% in GISAID. The proportion of Gamma variant was the highest in April (5.1%, 2/39) and decreased to 1.4% (2/141) and 1.2% (3/259) in May and June, respectively, in the imported SARS-CoV-2 surveillance. In GISAID, the proportion of Gamma variant was 5.9% (26,530/449,653) in April, which increased to 7.5% (25,933/347,752) in May, and reached a maximum of 7.9% (22,660/285,518) in June.

To assess the sensitivity of the surveillance, the time of each VOC for sample collection of the first record, the initial local transmission in the mainland of China as well as its designation by the WHO as a VOC were recorded (Table 1). The time intervals for Alpha, Delta, and Omicron variants between sample collection of their first record in the surveillance and WHO designation were less than one month. Except for Gamma, the time period for the remaining VOCs causing local transmission in the mainland of China was later than that of the sample collection of their first records in the surveillance. There was no local transmission caused by the Gamma variant in the mainland of China.

CONCLUSIONS

This study analyzed SARS-CoV-2 genomic sequence surveillance data from imported cases in the mainland of China in 2021. The 29 provincial CDCs with the submission of sequences performed well overall in terms of the number and timeliness of sequence submissions, but with different characteristics.

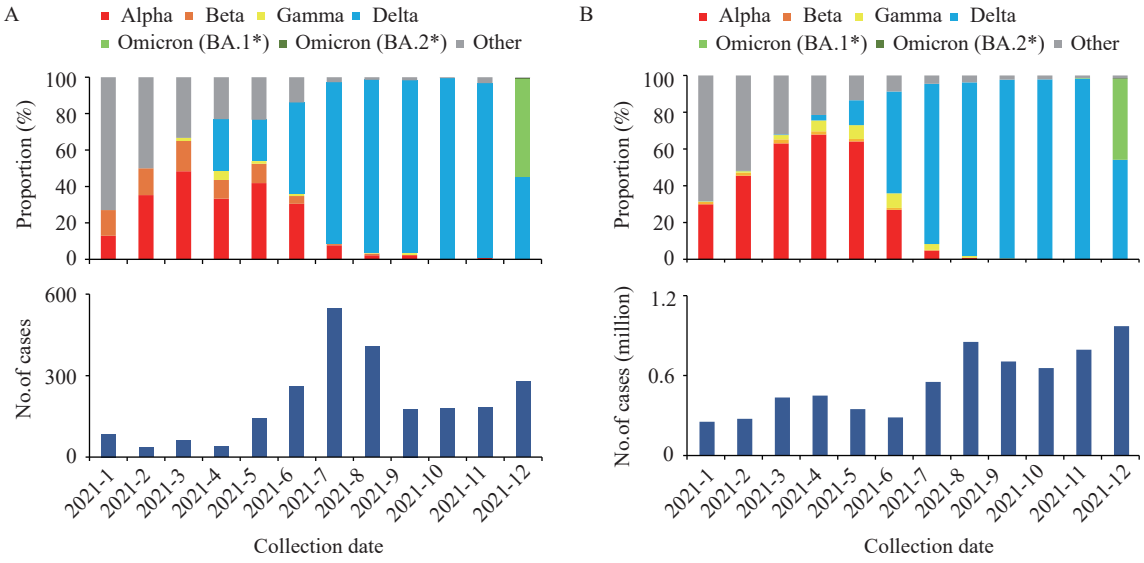

FIGURE 2. The proportion of SARS-CoV-2 VOCs in the imported SARS-CoV-2 surveillance and in GISAID, 2021. (A) The imported SARS-CoV-2 surveillance in the mainland of China (Data as of December 31, 2021). (B) GISAID (Data as of March 19, 2022).
Abbreviation: SARS-CoV-2=severe acute respiratory syndrome coronavirus 2; VOC=variant of concern; GISAID=the Global Initiative of Sharing All Influenza Data.

TABLE 1. The detection of SARS-CoV-2 VOCs in the mainland of China and the world.

VOC	Earliest recorded sequence in the imported SARS-CoV-2 surveillance		Date of first local transmission	Earliest documented samples in the world†	Date of designation by the WHO†
	Submitted PLAD	Submission date			
Alpha	Shanghai	2020-12-25 (Collection date: 2020-12-14)	Beijing, 2021-1-17	United Kingdom, 2020-9	VOC: 2020-12-18
Beta	Hunan	2021-2-7 (Collection date: 2021-1-16)	Guangdong, 2021-1-23	South Africa, 2020-5	VOC: 2020-12-18
Gamma	Jiangsu	2021-3-30 (Collection date: 2021-3-18)	–	Brazil, 2020-11	VOC: 2021-1-11
Delta	Chongqing	2021-4-28 (Collection date: 2021-4-22)	Guangdong, 2021-5-21	India, 2020-10	VOI: 2021-4-4 VOC: 2021-5-11
Omicron (BA.1*)	Tianjin	2021-12-13 (Collection date: 2021-12-9)	Guangdong, 2021-12-16	Multiple countries, 2021-11	VUM: 2021-11-24 VOC: 2021-11-26
Omicron (BA.2*)	Guangdong	2021-12-29 (Collection date: 2021-12-27)	Tianjin, 2022-2-26		

* Includes the descendent lineages.
† According to the official information published by the World Health Organization (*4*).
Abbreviation: SARS-CoV-2=severe acute respiratory syndrome coronavirus 2; WHO=World Health Organization; VOC=variant of concern; VOI=variant of interest; VUM=variant under monitoring; PLAD=provincial-level administrative division.

Notably, the number of sequence submissions is affected by at least two factors. The first was the number of imported cases. In this regard, Shanghai and Guangdong were the main ports of entry for the mainland of China (*11*), while Yunnan shares a border with Myanmar and has frequent personnel exchanges. Therefore, these PLADs had a high proportion of imported cases. The second was the viral load of the samples. In general, it is difficult to obtain the viral genome from samples with Ct values higher than 35 (*12*).

The epidemic trend from Alpha to Delta to Omicron in imported cases was consistent with that in GISAID. However, the proportions of Beta and Gamma variants imported to the mainland of China were different from those in GISAID, which may be affected in two ways. First, the data in GISAID may be influenced by differences in sampling strategies, sequencing capacities, and data-sharing time between countries (*13*). In contrast to the Alpha, Delta, and Omicron variants that were globally prevalent, Beta and Gamma variants were mostly prevalent in Africa and South America, respectively (*14*). The relatively low number of uploaded sequences in some African countries may explain the low prevalence of Beta variants in GISAID. Second, surveillance data should be interpreted with consideration of the limitations, including the difference in international communication, the number of imported cases, sequence submission, and sequencing capacities between PLADs.

Our data showed that the detection of VOCs in imported cases usually occurred after the WHO designation and before the time of local transmission. Early detection of imported vital variants is helpful for timely adjustment of prevention and control strategies and research. Many countries, including China, have strengthened their genomic surveillance to track the emergence of new VOCs in 2021 (*15*–*16*). However, since 2022, several countries have changed their testing strategies, leading to a decrease in the number of sequences shared with GISAID (*17*). This may have affected the early detection of new VOCs worldwide. The data in this study provides scientific support for strengthening the surveillance of imported SARS-CoV-2 in the mainland of China.

Conflicts of interest: No conflicts of interest.

Funding: National Key Research and Development Program of China (2021YFC0863000).

doi: 10.46234/ccdcw2022.144

Corresponding authors: Cao Chen, chencao@ivdc.chinacdc.cn; Wenbo Xu, xuwb@ivdc.chinacdc.cn.

[1] National Institute for Viral Disease Control and Prevention, Chinese Center for Disease Control and Prevention, Beijing, China; [2] National Health Commission Key Laboratory for Medical Virology and Viral Diseases, Beijing, China.
[&] Joint first authors.

Submitted: July 25, 2022; Accepted: August 03, 2022

REFERENCES

1. Peacock TP, Penrice-Randal R, Hiscox JA, Barclay WS. SARS-CoV-2 one year on: evidence for ongoing viral adaptation. J Gen Virol 2021;102(4):001584. http://dx.doi.org/10.1099/jgv.0.001584.
2. Chavda VP, Patel AB, Vaghasiya DD. SARS-CoV-2 variants and vulnerability at the global level. J Med Virol 2022;94(7):2986 – 3005. http://dx.doi.org/10.1002/jmv.27717.
3. Tao KM, Tzou PL, Nouhin J, Gupta RK, de Oliveira T, Pond SLK, et al. The biological and clinical significance of emerging SARS-CoV-2 variants. Nat Rev Genet 2021;22(12):757 – 73. http://dx.doi.org/10.1038/s41576-021-00408-x.
4. World Health Organization. Tracking SARS-CoV-2 variants. 2022. https://www.who.int/en/activities/tracking-SARS-CoV-2-variants/. [2022-8-2].
5. Ma HL, Zhang JQ, Wang J, Qin Y, Chen C, Song Y, et al. COVID-19 outbreak caused by contaminated packaging of imported cold-chain products — Liaoning Province, China, July 2020. China CDC Wkly 2021;3(21):441 – 7. http://dx.doi.org/10.46234/ccdcw2021.114.
6. Ma HL, Wang ZG, Zhao X, Han J, Zhang Y, Wang H, et al. Long distance transmission of SARS-CoV-2 from contaminated cold chain products to humans — Qingdao City, Shandong Province, China, September 2020. China CDC Wkly 2021;3(30):637 – 44. http://dx.doi.org/10.46234/ccdcw2021.164.
7. Chen C, Feng YN, Chen ZX, Xia Y, Zhao X, Wang J, et al. SARS-CoV-2 cold-chain transmission: characteristics, risks, and strategies. J Med Virol 2022;94(8):3540 – 7. http://dx.doi.org/10.1002/jmv.27750.
8. Zhou L, Nie K, Zhao HT, Zhao X, Ye BX, Wang J, et al. Eleven COVID-19 outbreaks with local transmissions caused by the imported SARS-CoV-2 delta VOC — China, July–August, 2021. China CDC Wkly 2021;3(41):863 – 8. http://dx.doi.org/10.46234/ccdcw2021.213.
9. Cheng C, Wang L, Lyu ZQ, Peng B, Li YH, Kong DF, et al. Four COVID-19 cases of new variant B.1.351 first emerging in South Africa in Chinese passengers on same flight — Shenzhen, China, January 2021. China CDC Wkly 2021;3(8):175 – 7. http://dx.doi.org/10.46234/ccdcw2021.049.
10. O'Toole Á, Scher E, Underwood A, Jackson B, Hill V, McCrone JT, et al. Assignment of epidemiological lineages in an emerging pandemic using the pangolin tool. Virus Evol 2021;7(2):veab064. http://dx.doi.org/10.1093/ve/veab064.
11. Civil Aviation Administration of China. 2021 statistical bulletin of civil airport development in China. 2022. http://www.caac.gov.cn/XXGK/XXGK/TJSJ/202203/t20220322_212478.html. [2022-8-2]. (In Chinese).
12. World Health Organization. Genomic sequencing of SARS-CoV-2: a guide to implementation for maximum impact on public health. 2021. https://www.who.int/publications/i/item/9789240018440. [2022-8-2].
13. GISAID. hCoV-19 submission tracker. 2022. https://gisaid.org/submission-tracker-global/. [2022-8-2].
14. GISAID. Tracking of variants. 2022. https://www.gisaid.org/hcov19-variants/. [2022-8-2].
15. Rego N, Costábile A, Paz M, Salazar C, Perbolianachis P, Spangenberg L, et al. Real-time genomic surveillance for SARS-CoV-2 variants of concern, Uruguay. Emerg Infect Dis 2021;27(11):2957 – 60. http://dx.doi.org/10.3201/EID2711.211198.
16. Paul P, France AM, Aoki Y, Batra D, Biggerstaff M, Dugan V, et al. Genomic surveillance for SARS-CoV-2 variants circulating in the United States, December 2020-May 2021. MMWR Morb Mortal Wkly Rep 2021;70(23):846 – 50. http://dx.doi.org/10.15585/mmwr.mm7023a3.
17. World Health Organization. Weekly epidemiological update on COVID-19 - 11 May 2022. 2022. https://www.who.int/publications/m/item/weekly-epidemiological-update-on-covid-19---11-may-2022. [2022-8-2].

Methods and Applications

Modeling Cross-Regional Transmission and Assessing the Effectiveness of Restricting Inter-Regional Population Movements in Controlling COVID-19 — Xi'an City, Shaanxi Province, China, 2021

Tianlong Yang[1,&]; Yao Wang[2,&]; Nankun Liu[3]; Guzainuer Abudurusuli[1]; Shiting Yang[1]; Shanshan Yu[1]; Weikang Liu[1]; Xuecheng Yin[4]; Tianmu Chen[1,2,#]

ABSTRACT

Introduction: The aim of this study was to construct an assessment method for cross-regional transmission of coronavirus disease 2019 (COVID-19) and to provide recommendations for optimizing measures such as interregional population movements.

Methods: Taking Xi'an City as the example subject of this study's analysis, a Cross-Regional-Gravitational-Dynamic model was constructed to simulate the epidemic in each district of Xi'an under three scenarios of controlled population movement (Scenario 1: no intensive intervention; Scenario 2: blocking Yanta District on December 18 and blocking the whole region on December 23; and Scenario 3: blocking the whole region on December 23). This study then evaluated the effects of such simulated population control measures.

Results: The cumulative number of cases for the three scenarios was 8,901,425, 178, and 474, respectively, and the duration of the epidemic was 175, 18, and 22 days, respectively. The real world prevention and control measures in Xi'an reduced the cumulative number of cases for its outbreak by 99.98% in comparison to the simulated response in Scenario 1; in contrast, the simulated prevention and control strategies set in Scenarios 2 (91.26%) and 3 (76.73%) reduced cases even further than the real world measures used in Xi'an.

Discussion: The constructed model can effectively simulate an outbreak across regions. Timely implementation of two-way containment and control measures in areas where spillover is likely to occur is key to stopping cross-regional transmission.

INTRODUCTION

The global spread of mutant strains is the main reason why coronavirus disease 2019 (COVID-19) is difficult to control. In March 2022, the subtype mutant strain BA.2 of Omicron was found in localized cases in at least 9 regions of China (such as Jilin Province, Shanghai Municipality, Fujian Province, etc.). Due to its insidious nature and rapid transmission (*1*–*2*), a large number of widely dispersed cases emerged in a short period of time. This posed a great risk of spillover to surrounding areas and made it extremely difficult for China to achieve its goal of maintaining a dynamic 'COVID-zero' policy.

By reviewing our previously constructed COVID-19 transmission dynamics models, we found that most studies have only focused on assessing the spread of COVID-19 within the overall region (*3*–*7*), and failed to consider the differences in control strategies among regions in cross-regional transmission epidemics. This could easily lead to misjudgment of the division of blockade control areas, thus causing unnecessary economic losses and the wastage of health resources. The dynamical mechanism of cross-regional transmission is consistent with the spatial decay characteristics of the gravitational model (*8*), i.e., where spatial spread is proportional to size and inversely proportional to distance. Therefore, constructing a cross-regional transmission model and considering interregional population movement to simulate morbidity trends are helpful in achieving China's political goal through supporting multi-regional joint prevention and control.

In this study, a cross-region transmission epidemic in Xi'an City, Shaanxi Province in December 2021 was selected as the research case to analyze the characteristics of core-peripheral vertical spread in the Yanta District of Xi'an, and to assess the effect of population movement containment among regions in different outbreak periods, through constructing a Cross-Regional-Gravitational-Dynamic model (CRGD).

METHODS

Data Collection

Data on reported cases from December 9, 2021, to January 20, 2022, were collected from the website of the Shaanxi Provincial Health Commission (http://sxwjw.shaanxi.gov.cn/). Demographic data and geographical distribution data were obtained from the Shaanxi Provincial Statistical Yearbook (http://tjj.shaanxi.gov.cn/upload/2021/zk/indexch.htm).

Model Framework

The inter-regional transmission mechanism of COVID-19 from Yanta District to its surrounding areas is similar to the attractiveness between a place and other surrounding places as described by the local gravity model. This study combined the transmission dynamics model with the local gravity model and used the Susceptible-Exposed-Infectious-Recovered (SEIR) model to form the overall framework of COVID-19 propagation. It adjusted relevant parameters according to the definition of the local gravity model (Figure 1). Specifically, our model is based on the following assumptions: 1) Only cross-regional transmission from Yanta District to other districts was considered, with consistent transmission across districts and different cross-regional transmission excluded; 2) The model divides the population into susceptible persons a (S_a), exposed persons a (E_a), infectious persons a (I_a), and recovered persons a (R_a) in Yanta District and susceptible persons i (S_i), exposed persons i (E_i), infectious persons i (I_i), and recovered persons i (R_i) in other districts; 3) The coefficients of transmission rate in other regions and Yanta District are β_i and β_a, respectively. The coefficient of transmission rate across regions is β_{ai}; 4) ω is the latent coefficient; 5) Symptomatic patients are defined as removed persons after an infectious period of $1/\gamma$; 6) Natural births, deaths, and deaths after illness of the population are not considered in this model for a short time outbreak.

The equations of the model are as follows:

$$\frac{dS_a}{dt} = -\beta_a S_a I_a \quad (1)$$

$$\frac{dE_a}{dt} = \beta_a S_a I_a - \omega E_a \quad (2)$$

$$\frac{dI_a}{dt} = \omega E_a - \gamma I_a \quad (3)$$

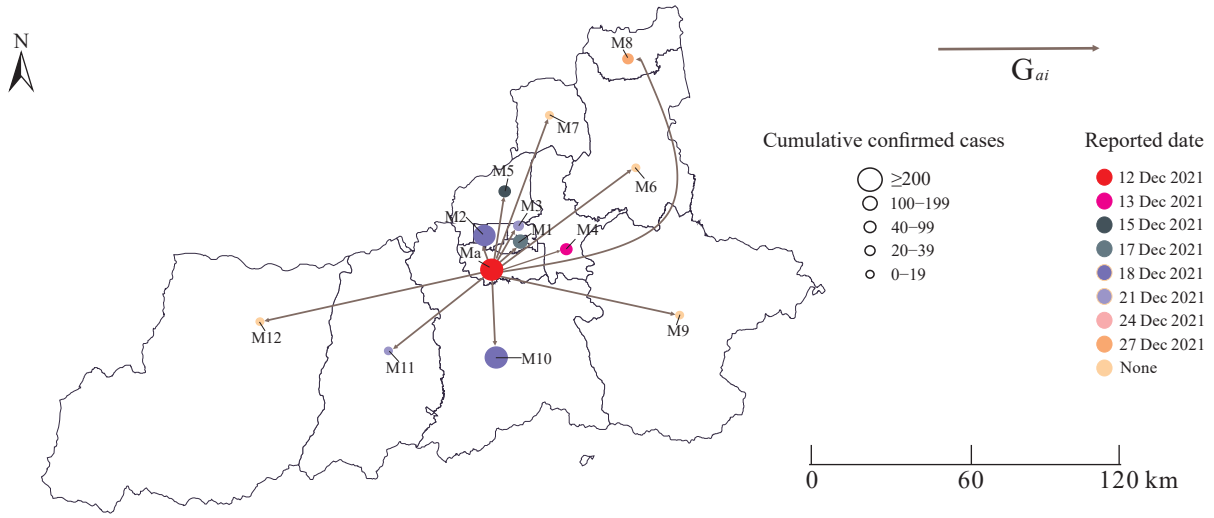

FIGURE 1. CRGD model framework of COVID-19 in Xi'an City.
Note: The arrows in the figure denote the transmission coefficient of Yanta District spreading to the surrounding areas, indicated by G_{ai}, $G_{ai} = \int (N_{ai} \cdot K_{ai} \cdot c) = \beta_{ai} = \beta_a \times \frac{N_a \times N_i}{K_i} \times c$; N_a denotes the number of residents in Yanta District, N_i denotes the number of residents in other districts, K_i denotes the distance between Yanta District and each other district, and c is a constant, β_{ai} is proportional to the population size and inversely proportional to the distance, a denotes Yanta District, i denotes other districts. Circle M denotes SEIR model, the size of the circle denotes the number of cases in this district, and the number (or a) after M denotes for Districts (a: Yanta District; 1: Beilin District; 2: Lianhu District; 3: Xincheng District; 4: Baqiao District; 5: Weiyang District; 6: Lintong District; 7: Gaoling District; 8: Yanliang District; 9: Lantian County; 10: Chang'an District; 11: Huyi District; 12: Zhouzhi County).
Abbreviation: COVID-19=coronavirus disease 2019; CRGD=Cross-Regional-Gravitational-Dynamic; SEIR=susceptible-exposed-infectious-recovered.

$$\frac{dR_a}{dt} = \gamma I_a \quad (4)$$

$$\frac{dS_i}{dt} = -\beta_i S_i I_i - \beta_{ai} S_i I_a \quad (5)$$

$$\frac{dE_i}{dt} = \beta_i S_i I_i + \beta_{ai} S_i I_a - \omega E_i \quad (6)$$

$$\frac{dI_i}{dt} = \omega E_i - \gamma I_i \quad (7)$$

$$\frac{dR_i}{dt} = \gamma I_i \quad (8)$$

The values of the parameters in this study were taken from previous studies (*9*). We set the parameter of ω to 0.5, the parameter γ to 0.3 (*10*), and the parameters β_i, β_a, and β_{ai} were set from fitting and extrapolating the actual data.

Pre- and Post-Intervention Cross-Regional Transmission Coefficients

β_{ai} denotes the transmission coefficient of Yanta District spreading to the surrounding areas. Before the intervention, it conforms to the decay law of the gravity model (G_{ai}) representing disease transmission, i.e., β_{ai} is proportional to the population size and inversely proportional to the distance. β_{ai} is calculated as follows: N_a denotes the number of residents in Yanta District, N_i denotes the number of residents in other districts, K_i denotes the distance between Yanta District and each other district, and c is a constant. After the intervention, the cross-district transmission is blocked and β_{ai} is 0.

$$G_{ai} = \int (N_{ai} \cdot K_{ai} \cdot c) = \beta_{ai} = \beta_a \times \frac{N_a \times N_i}{K_i} \times c \quad (9)$$

Pre- and Post-Intervention Intra-Regional Transmission Coefficients

Before the intervention, β_i is calculated by fitting actual reported data and transmission dynamics model curves. After the intervention, according to previous studies, the most effective prevention and control of the outbreak can be achieved when the transmissibility is reduced by 50% (*5*), accelerating the end of the epidemic. It is therefore assumed that the transmissibility within each district can be reduced by a factor of 50 after the intervention, as follows:

$$\beta_i' = \beta_i/50 \quad (10)$$

Quantitative Evaluation of Transmissibility

According to a previous study (*6*), the effective reproductive number (R_{eff}) can be used as an indicator to assess the transmissibility of COVID-19, as follows:

$$R_{eff_{i/ai}} = \frac{\beta_{i/ai} \times S_i}{\gamma} \quad (11)$$

Scenario Setting

Three scenarios were hypothesized and simulated using the constructed model based on the possible time points for implementing prevention and control strategies for this outbreak in Xi'an. Scenario 1 is no intervention in all districts of Xi'an; Scenario 2 is a lockdown measure for all districts in the city on December 23 following lockdown measures for Yanta District on December 18; and Scenario 3 is a lockdown measure for all districts in the city on December 23. We used the software Berkeley Madonna (version 8.3.18, Copyright©1993–2001 Robert I. Macey & George F. Oster and developed by Robert Macey and George Oster of the University of California at Berkeley in USA.) to perform the curve fitting and simulation.

Global Spatial Autocorrelation Analysis

OpenGeoDa software (version 1.2.0, Copyright© 2011–2020 Luc Anselin & Mark McCann and developed by Arizona State University, Phoenix, AZ, US) was used to calculate the global Moran's I coefficient and detect the overall spatial autocorrelation. The range of Moran's I coefficient is [–1, 1]. When the value is greater than 0, the spatial correlation is positive: the larger the value, the stronger the spatial clustering. When the value is less than 0, the spatial correlation is negative. The closer the value is to –1, the greater the spatial difference (the space itself is irrelevant). Of note, the significance of Moran's I coefficient is based on the Z and P values.

RESULTS

From December 12, 2021 to January 13, 2022, there were 2,037 cases of this outbreak in Xi'an, and the outbreak lasted for 32 days. The outbreak involved a total of 11 districts. It was largely attributed to an intra-district spread in the Yanta District of Xi'an from December 10 to 18, 2021 before spreading to other areas of the city after December 18, 2021. According to the fitted and calculated equations, the coefficients of transmission rates and R_{eff} within and across districts of Xi'an city without intensive interventions (Supplementary Table S1, available in http://weekly.

chinacdc.cn/).

The assumptions of Scenario 1 resulted in a much larger outbreak of the epidemic than what actually occurred in real life. Scenario 1 simulated epidemic peaked on January 30, 2022, with a peak population of 493,212 cases, and the epidemic lasted for 175 days, ending on June 5, 2022. The cumulative number of simulated cases reached approximately 8,901,425. In other words, Scenario 1 was shown to be 99.98% less effective than the comprehensive prevention and control measures actually used in the real world Xi'an outbreak.

The assumptions of Scenario 2 resulted in a much smaller outbreak of the epidemic than what actually occurred in real life. Scenario 2 simulation results indicated that the epidemic in Xi'an would have peaked on December 23, 2021, with a peak number of 20 cases and an epidemic duration of 18 days, and would have ended on December 30, 2021, with a cumulative number of 178 cases. This represents a 91.26% reduction in the cumulative number of cases compared to the real world epidemic situation in Xi' an. In this simulated scenario, there were also no cases predicted to appear in Baqiao District, Huyi District, Lintong District, Xincheng District, or Yanliang District.

The assumptions of Scenario 3 resulted in a much smaller outbreak of the epidemic than what actually occurred in Xi'an in real life, although still showed a larger outbreak than Scenario 2. Scenario 3 assumed that if all areas of Xi'an were in direct lockdown on December 23, 2021, then this outbreak would be in all districts of the city on December 23, 2021. According to the results of this simulation, the epidemic in Xi'an would have peaked on December 23, 2021, with a peak number of 85 cases. The duration of the epidemic would have been 22 days, and the cumulative number of cases would have been 474 at the end of the epidemic on January 3, 2022. This simulated prevention and control strategy reduced the cumulative number of cases by 76.73% compared to the real world epidemic situation in Xi'an. In this simulated scenario, there were also no cases predicted to appear in Huyi District, Lintong District, or Yanliang District.

The epidemiological situations for the above three scenarios are shown in Table 1, Figure 2, and Figure 3.

The global Moran's I coefficients for COVID-19 in Xi'an from December 12, 2021 to January 13, 2022, were not significantly different (P>0.05), and the COVID-19 distribution showed no spatial correlation across the districts (Supplementary Table S2, available in http://weekly.chinacdc.cn/).

DISCUSSION

The cross-regional transmission model constructed in this study provides a method to assess the likelihood and epidemic scale of regional cluster outbreaks to neighboring regions based on previous transmission dynamic models as well as incorporates the local gravitational effects of disease transmission. The current epidemic status and containment scale of COVID-19 vary among countries, and modeling the impact of a new epidemic in one region on other regions allows relevant authorities to prepare medical stockpiles in advance to deal with epidemics in other countries. This assessment method can thus provide ideas for inter-regional movement and transmission of diseases, and provide a theoretical basis for the prevention and control of endemic diseases.

Combining the results of the incidence map and the global autocorrelation analysis in Xi'an, we found no spatial correlation between the differences in COVID-19 incidence in the various districts of Xi'an, implying that the cases were randomly distributed across the districts without regional aggregation. This suggested that cases were effectively managed and isolated between most districts in the early stages of the outbreak in Xi'an. Outbreaks in other districts were due to transmission and spread of individual cases from the Yanta District into the district resulting in transmission within the district, which is consistent with the simulation results of the CRGD model — where the transmissibility from the Yanta District into other districts was less than 1 and the transmissibility within each district was more than 1. The real world epidemiological response in Xi'an reduced the number of cases by 99.98% and the duration of the epidemic by 175 days compared to Scenario 1, indicating that the comprehensive interventions implemented in Xi'an were effective. However, Scenario 2 and Scenario 3 could reduce the cumulative number of cases by a further 91.26% and 76.73%, respectively, compared to the outbreak in real life. This indicates that if the first source of the epidemic (Yanta District) had been blocked in time at the beginning of the epidemic, the scale of the further spread of epidemic could have been better prevented and the expected effect of preventing and controlling the epidemic could have been achieved. Also, if intra- and inter-regional transmission had been strictly controlled and blocked in all areas on December 23, 2021, it would have had a better control

TABLE 1. Epidemiological results of interventions in Xi'an City and its sub-districts under three scenarios.

Scenario	Area	Cumulative number of cases	Cumulative attack rate (%)	Lasting time (days)	Time of peak number of cases (m/d/y)	Peak number of cases
Scenario 1	Xi'an City	8,901,425	68.721	175	1/30/2022	493,212
	Yanta District	1,880,632	91.783	109	1/30/2022	117,349
	Baqiao District	732,590	71.752	131	2/4/2022	35,512
	Beilin District	603,768	79.653	112	2/1/2022	34,201
	Huyi District	108,750	18.847	163	2/6/2022	3,909
	Lianhu District	907,175	89.026	108	1/30/2022	55,058
	Lintong District	213,623	31.601	170	2/7/2022	7,554
	Weiyang District	1,472,621	94.641	105	1/28/2022	95,543
	Xixian New Area	1,088,536	83.438	120	2/2/2022	60,107
	Xincheng District	402,634	65.151	117	2/2/2022	20,984
	Yanliang District	11,066	3.652	106	2/4/2022	510
	Chang'an District	1,479,973	93.315	106	1/29/2022	94,778
Scenario 2	Xi'an City	178	0.001	18	12/23/2021	20
	Yanta District	38	0.002	11	12/18/2021	7
	Baqiao District	–	–	–	–	–
	Beilin District	3	0.001	7	12/18/2021	1
	Huyi District	–	–	–	–	–
	Lianhu District	17	0.002	13	12/23/2021	2
	Lintong District	–	–	–	–	–
	Weiyang District	48	0.003	16	12/23/2021	7
	Xixian New Area	10	0.001	13	12/23/2021	2
	Xincheng District	–	–	–	–	–
	Yanliang District	–	–	–	–	–
	Chang'an District	38	0.002	16	12/23/2021	6
Scenario 3	Xi'an City	474	0.004	22	12/23/2021	85
	Yanta District	155	0.008	19	12/23/2021	26
	Baqiao District	13	0.001	14	12/23/2021	3
	Beilin District	23	0.003	15	12/23/2021	5
	Huyi District	–	–	–	–	–
	Lianhu District	47	0.005	16	12/23/2021	9
	Lintong District	–	–	–	–	–
	Weiyang District	101	0.007	18	12/23/2021	20
	Xixian New Area	24	0.002	15	12/23/2021	5
	Xincheng District	10	0.002	13	12/23/2021	2
	Yanliang District	–	–	–	–	–
	Chang'an District	80	0.005	18	12/23/2021	16

Note: "–" means no data.

effect than how it spread in real life without these controls. This suggests that the implementation of outbreak control in Xi'an needs further improvement, and that timely two-way blockade control measures in the outbreak regions and potential spillover areas are key to avoiding cross-regional transmission. As such, these findings provide a compelling control strategy for avoiding cross-regional transmission in other areas in the future.

There were some limitations to this study. First, the

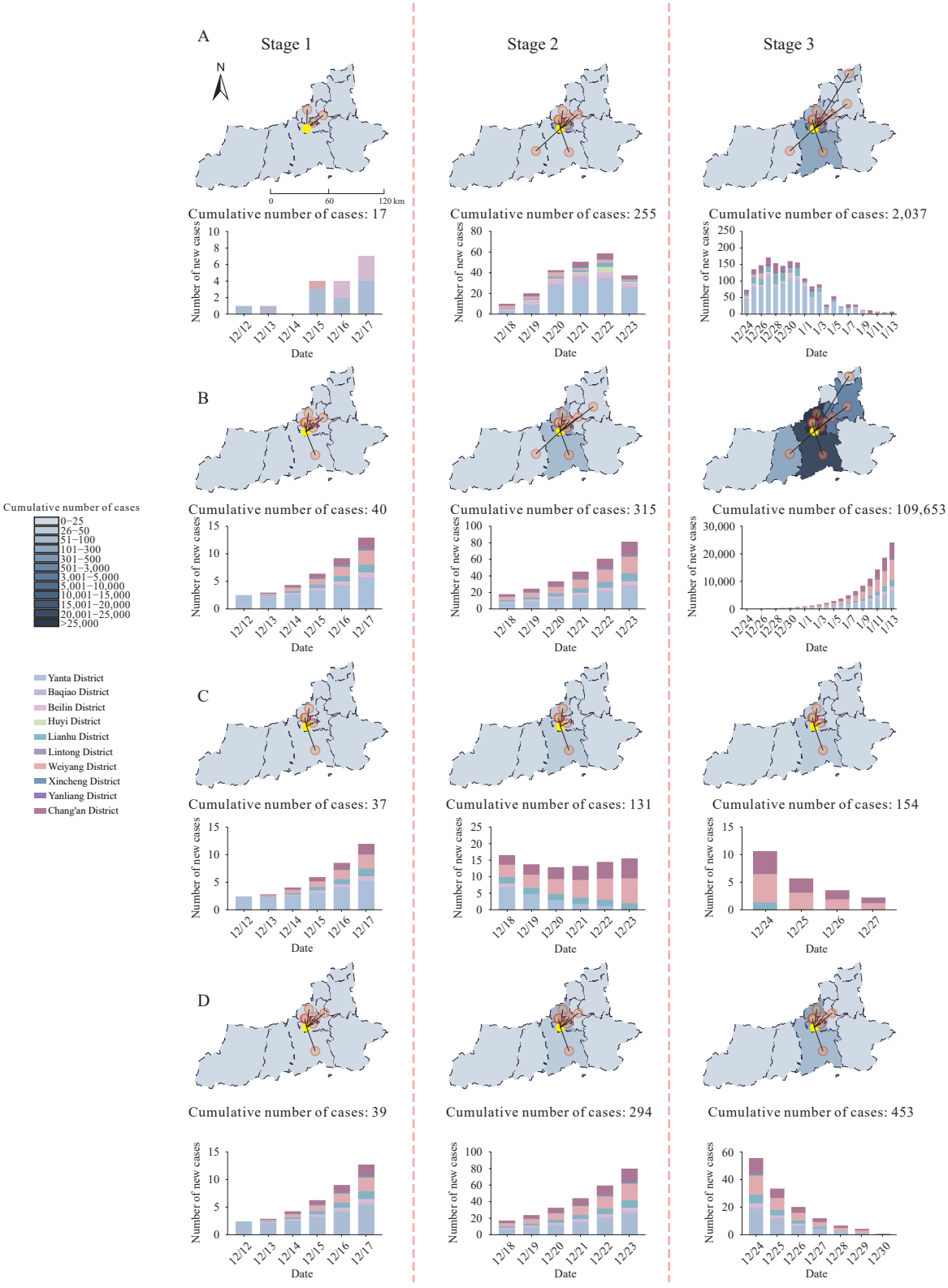

FIGURE 2. Changes in cases at different stages of prevention and control in various districts of Xi'an under different scenarios. (A) Actual scenario; (B) Scenario 1; (C) Scenario 2; (D) Scenario 3.
Note: The trend of this epidemic is divided into 3 stages (Stage 1: before December 18, 2021; Stage 2: from December 18 to 23, 2021; Stage 3: after December 23, 2021). The yellow circle denotes the area where the COVID-19 outbreak started — Yanta District. Other circles denote the spread of COVID-19 from the Yanta district to other areas thereby causing other regional spread.

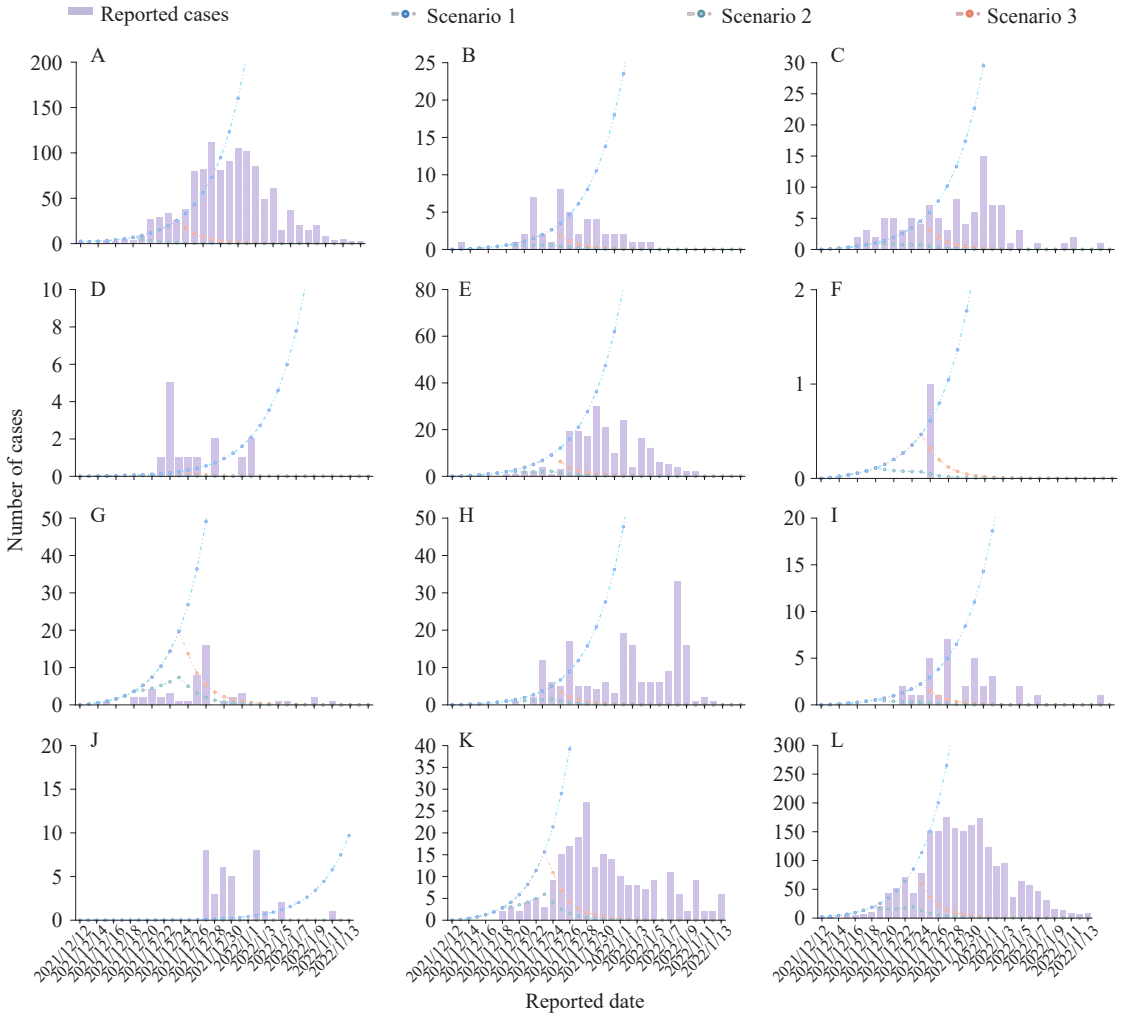

FIGURE 3. Curves of epidemic of different scenarios in Xi'an City and it's sub-districts. (A) Yanta District; (B) Baqiao District; (C) Beilin District; (D) Huyi District; (E) Lianhu District; (F) Lintong District; (G) Weiyang District; (H) Xixian New Area; (I) Xincheng District; (J) Yanliang District; (K) Chang'an District; (L) Xi'an District.

number of cases collected in this paper was calculated based on the reported date, and thus may have overestimated the transmissibility of the district at the beginning of the outbreak by ignoring the occult transmission that had already occurred before the report. Second, since cross-transmission between districts is less likely after the adoption of blockade control in each district, this study only considered the spread of the disease from Yanta District to other districts; cross-transmission between other districts was not considered in this study, which may have overestimated the cross-district spread of the disease in Yanta District. Finally, future studies should also measure spatial stratified heterogeneity (SSH) to further interrogate the inter-regional transmission pattern of this and similar outbreaks (*11–12*). However, in terms of this study, a lack of detailed case locations due to data quality limitations would have led to spatial applicability issues in assessing epidemiological spatial distribution for the simulation results of the three scenarios selected for this study in particular, which is why SSH was not included. However, as the aim of this study was to provide a methodological study of cross-regional transmission of the risk of spillover from the epidemic source to other areas, non-inclusion of SSH did not have a major impact on the construction of this model or its resulting simulations.

Conflicts of interest: No conflicts of interest.

Acknowledgements: Participants who provided the data and the field investigators who collected the data.

Funding: Supported by the National Key Research and Development Program of China (2021YFC2301604).

doi: 10.46234/ccdcw2022.143

Corresponding author: Tianmu Chen, 13698665@qq.com.

[1] School of Public Health, Xiamen University, Xiamen City, Fujian Province, China; [2] State Key Laboratory of Molecular Vaccinology and Molecular Diagnostics, Xiamen University, Xiamen City, Fujian Province, China; [3] Chinese Center for Disease Control and Prevention, Beijing, China; [4] School of Public Health, Yale University, New Haven, Connecticut, US.
[&] Joint first authors.

Submitted: May 10, 2022; Accepted: July 19, 2022

REFERENCES

1. Brandal LT, MacDonald E, Veneti L, Ravlo T, Lange H, Naseer U, et al. Outbreak caused by the SARS-CoV-2 Omicron variant in Norway, November to December 2021. Euro Surveill 2021;26(50):2101147. http://dx.doi.org/10.2807/1560-7917.ES.2021.26.50.2101147.
2. PHO. COVID-19 Omicron (B.1.1.529) Variant of Concern and Communicability … What We Know So Far. 2022. https://www.publichealthontario.ca/-/media/documents/ncov/covid-wwksf/2022/01/wwksf-omicron-communicability.pdf?sc_lang=en&_cldee=amxhbmdAc3dwdWJsaWNoZWFsdGguY2E%3D&recipientid=contact-91ec7f1fb2c2e41191f10050569e0009-0cbe3a8a0d0746bdba6e3afcb2d4d2a1&esid=4c00302f-8569-ec11-8ed8-0050569e118f%5bM. [2022-4-18]. (In Chinese).
3. Zhao QL, Wang Y, Yang M, Li MN, Zhao ZY, Lu XR, et al. Evaluating the effectiveness of measures to control the novel coronavirus disease 2019 in Jilin Province, China. BMC Infect Dis 2021;21(1):245. http://dx.doi.org/10.1186/s12879-021-05936-9.
4. Lao XY, Luo L, Lei Z, Fang T, Chen Y, Liu YH, et al. The epidemiological characteristics and effectiveness of countermeasures to contain coronavirus disease 2019 in Ningbo City, Zhejiang Province, China. Sci Rep 2021;11(1):9545. http://dx.doi.org/10.1038/s41598-021-88473-4.
5. Liu WK, Ye WJ, Zhao ZY, Liu C, Deng B, Luo L, et al. Modelling the emerging COVID-19 epidemic and estimating intervention effectiveness - Taiwan, China, 2021. China CDC Wkly 2021;3(34):716 – 9. http://dx.doi.org/10.46234/ccdcw2021.177.
6. Zhao QL, Yang M, Wang Y, Yao LS, Qiao JG, Cheng ZY, et al. Effectiveness of interventions to control transmission of reemergent cases of COVID-19 - Jilin Province, China, 2020. China CDC Wkly 2020;2(34):651 – 4. http://dx.doi.org/10.46234/ccdcw2020.181.
7. Chen TM, Rui J, Wang QP, Zhao ZY, Cui JA, Yin L. A mathematical model for simulating the phase-based transmissibility of a novel coronavirus. Infect Dis Poverty 2020;9(1):24. http://dx.doi.org/10.1186/s40249-020-00640-3.
8. Chen YG, Li YJ, Feng S, Man XM, Long YQ. Gravitational scaling analysis on spatial diffusion of COVID-19 in Hubei Province, China. PLoS One 2021;16(6):e0252889. http://dx.doi.org/10.1371/JOURNAL.PONE.0252889.
9. Zhao ZY, Niu Y, Luo L, Hu QQ, Yang TL, Chu MJ, et al. The optimal vaccination strategy to control COVID-19: a modeling study in Wuhan City, China. Infect Dis Poverty 2021;10(1):140. http://dx.doi.org/10.1186/s40249-021-00922-4.
10. Tang XJ, Musa SS, Zhao S, Mei SJ, He DH. Using proper mean generation intervals in modeling of COVID-19. Front Public Health 2021;9:691262. http://dx.doi.org/10.3389/fpubh.2021.691262.
11. Wang JF, Zhang TL, Fu BJ. A measure of spatial stratified heterogeneity. Ecol Indic 2016;67:250 – 6. http://dx.doi.org/10.1016/j.ecolind.2016.02.052.
12. Hu BS, Ning P, Qiu JY, Tao V, Devlin AT, Chen HY, et al. Modeling the complete spatiotemporal spread of the COVID-19 epidemic in mainland China. Int J Infect Dis 2021;110:247 – 57. http://dx.doi.org/10.1016/j.ijid.2021.04.021.

Supplementary Material

SUPPLEMENTARY TABLE S1. Coefficients for transmissibility and effective reproduction number within and across districts in Xi'an without intervention.

District	β_i	R_{eff_i}	β_{ai}	$R_{eff_{ai}}$
Yanta District	4.43×10^{-7}	2.72	–	–
Baqiao District	4.43×10^{-7}	2.72	5.15×10^{-8}	0.16
Beilin District	4.43×10^{-7}	2.72	1.40×10^{-7}	0.32
Fuyi District	4.43×10^{-7}	2.72	1.14×10^{-8}	0.02
Lianhu District	4.43×10^{-7}	2.72	1.78×10^{-7}	0.54
Lintong District	4.43×10^{-7}	2.72	1.70×10^{-8}	0.03
Weiyang District	4.43×10^{-7}	2.72	1.72×10^{-7}	0.80
Xixian New Area	4.43×10^{-7}	2.72	6.23×10^{-8}	0.24
Xincheng District	4.43×10^{-7}	2.72	9.20×10^{-7}	0.17
Yanliang District	4.43×10^{-7}	2.72	3.99×10^{-9}	0.01
Chang'an District	4.43×10^{-7}	2.72	1.31×10^{-7}	0.62

Note: "–" means reference.

SUPPLEMENTARY TABLE S2. Global autocorrelation of the incidence of COVID-19 in Xi'an City from December 12, 2021 to January 13, 2022.

Time	Moron's *I*	*Z*	*P*
Before December 18, 2021	−0.149	−0.583	0.330
December 18 to 23, 2021	−0.100	−0.168	0.438
After December 23, 2021	−0.025	0.442	0.284

Abbreviation: COVID-19=coronavirus disease 2019.

Notes from the Field

First Imported Case of SARS-CoV-2 Omicron Subvariant BA.2.12.1 — Guangdong Province, China, April 30, 2022

Lijun Liang[1,&]; Xiang Zhao[2,&]; Aiping Deng[1]; Kuibiao Li[3]; Jiajun Liu[1]; Fangzhu Ouyang[1]; Qianfang Guo[1]; Jing Xu[1]; Shen Huang[1]; Lirong Zou[1]; Yang Song[2]; Kai Nie[2,#]; Baisheng Li[1,#]

On April 23, 2022, an international flight KQ880 from Nairobi, Kenya arrived at Guangzhou Baiyun International Airport, Guangzhou City, Guangdong Province. All passengers were transferred to the quarantine hotel for routine 14-day medical observation and regularly tested of severe acute respiratory syndrome coronavirus 2 (SARS-CoV-2) nucleic acid. One of the patients, a 27-year-old Chinese male, reported positive SARS-CoV-2 nucleic acid on April 27, 2022. The patient had a history of full coronavirus disease 2019 (COVID-19) vaccination and denied exposure to other COVID-19 cases in the past 14 days. After diagnosis, he was transferred to Guangzhou Eighth People's Hospital for treatment.

On April 30, 2022, a nasal swab sample from the patient was sequenced using the Illumina MiniSeq platform (Illumina, San Diego, CA, USA), and genotyping results showed that the patient was infected with Omicron subvariant BA.2.12.1. A total of 33 amino acid mutation sites (T19I, A27S, G142D, V213G, G339D, S371F, S373P, S375F, T376A, D405N, R408S, K417N, N440K, L452Q, S477N, T478K, E484A, Q493R, Q498R, N501Y, Y505H, D614G, H655Y, N679K, P681H, S704L, N764K, D796Y, Q954H, N969K and L24del, P25del, P26del) were detected on the spike gene, two of which (L452Q and S704L) were key sites defining the signature of sublineage BA.2.12.1 (*1*–*2*) (Figure 1). The sequence has been submitted to the National Genomics Data Center (under the accession number WGS025539).

On May 4, 2022, the World Health Organization reminded to closely monitor BA.2.12.1 subvariant (*2*). Compared to other Omicron variants, BA.2.12.1 subvariant shows stronger immune escape, even after having been vaccinated with booster dose (*3*). Several studies have shown that the transmissibility of BA.2.12.1 is about 23% to 27% faster than that of BA.2. Omicron BA 2.12.1 subvariant spread very fast, which led to the resurgence of the epidemic in many parts of the United States, and cases have been reported in at least 17 countries (*4*). Public health officials are focusing on this subvariant and trying to learn more.

doi: 10.46234/ccdcw2022.094

Corresponding authors: Kai Nie, niekai@ivdc.chinacdc.cn; Baisheng Li, libsn@126.com.

[1] Guangdong Provincial Center for Disease Control and Prevention, Guangzhou City, Guangdong Province, China; [2] National Institute for Viral Disease Control and Prevention, China CDC, Beijing, China; [3] Guangzhou Center for Disease Control and Prevention, Guangzhou City, Guangdong Province, China.
& Joint first authors.

Submitted: May 11, 2022; Accepted: May 15, 2022

REFERENCES

1. Outbreak.info. SARS-CoV-2 (hCoV-19) mutation reports: lineage comparison. https://outbreak.info/compare-lineages?pango=BA.2.12.1&gene=S&threshold=0.2. [2022-5-2].
2. World Health Organization. COVID-19 weekly epidemiological update edition 90, published 4 May 2022. https://apps.who.int/iris/bitstream/handle/10665/353976/nCoV-weekly-sitrep4May22-eng.pdf?sequence=1&isAllowed=y. [2022-5-5].
3. Cao Y, Yisimayi A, Jian F, Song W, Xiao T, Wang L, et al. BA.2.12.1, BA.4 and BA.5 escape antibodies elicited by Omicron infection. bioRxiv 2022. http://dx.doi.org/10.1101/2022.04.30.489997.
4. Centers for Disease Control and Prevention. COVID data tracker. 2022, April 29. https://covid.cdc.gov/covid-data-tracker. [2022-5-5].

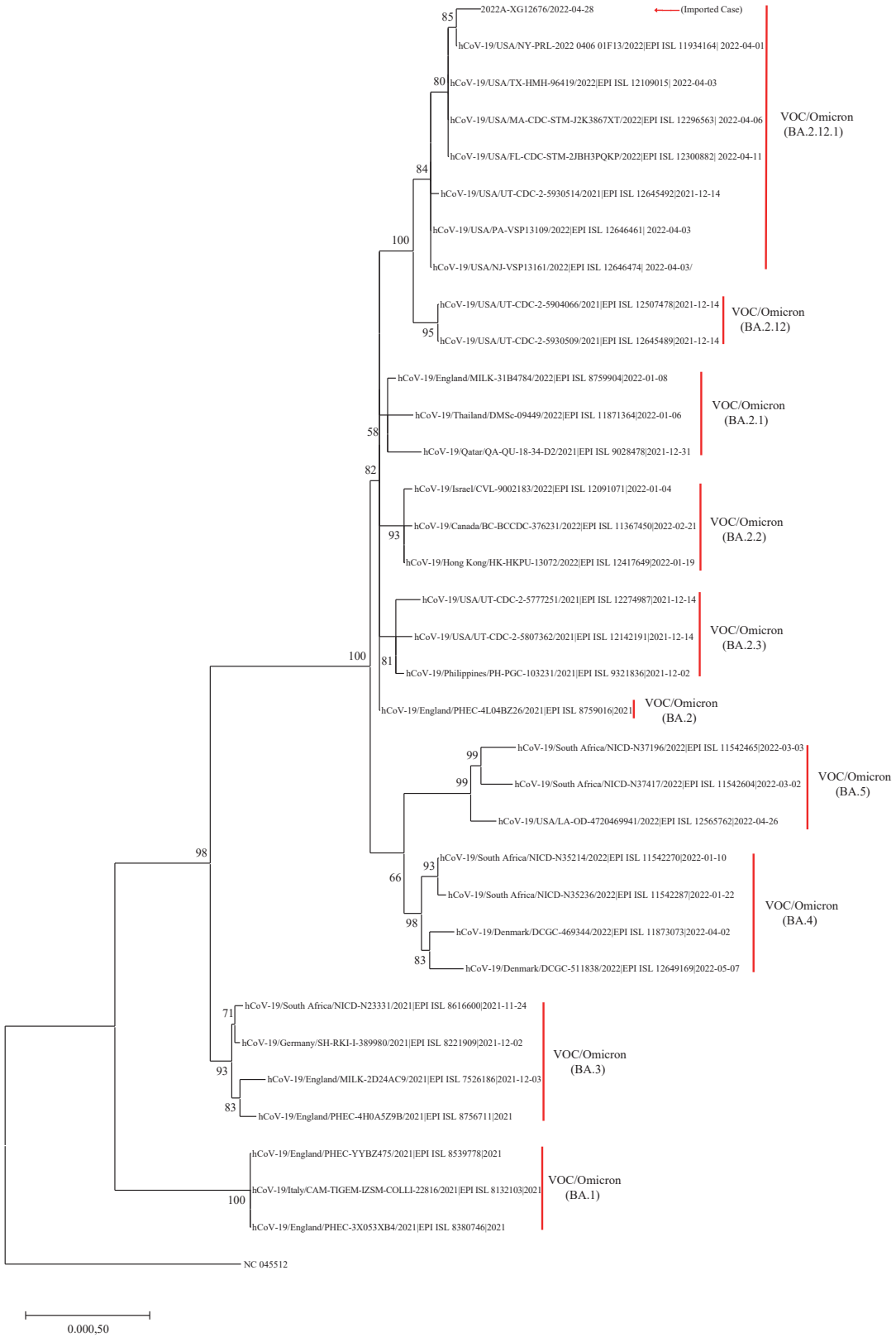

FIGURE 1. Phylogenetic tree based on the full-length genome sequences of the COVID-19 Omicron subvariants.
Note: Guangdong Province imported VOC/Omicron (BA.2.12.1) variant is indicated with red arrow. Other Omicron sublineages are indicated on the right side and marked with square brackets.
Abbreviation: COVID-19=coronavirus disease 2019; VOC=variant of concern.

Indexed by PubMed Central (PMC), Emerging Sources Citation Index (ESCI), Scopus, Chinese Scientific and Technical Papers and Citations, and Chinese Science Citation Database (CSCD)

The inauguration of *China CDC Weekly* is in part supported by Project for Enhancing International Impact of China STM Journals Category D (PIIJ2-D-04-(2018)) of China Association for Science and Technology (CAST).

CCDC weekly

Vol. 4 No. 31 Aug. 5, 2022

Responsible Authority
National Health Commission of the People's Republic of China

Sponsor
Chinese Center for Disease Control and Prevention

Editing and Publishing
China CDC Weekly Editorial Office
No.155 Changbai Road, Changping District, Beijing, China
Tel: 86-10-63150501, 63150701
Email: weekly@chinacdc.cn

CSSN
ISSN 2096-7071
CN 10-1629/R1